International Journal of Design & Nature and Ecodynamics
Vol. 20, No. 12, December, 2025, pp. 2949-2955
Journal homepage: http://iieta.org/journals/ijdne

Numerical Simulation of Lead-Free $Cs_2AgBiBr_6$ Double Perovskite Solar Cells: Performance Limits and Illumination Geometry Effects

Haneafa Yahya Najem[1], Raad A. Rasool[2], Asmaa Fareed Abdullateef Al Tayee[3], Ali M. Saadi[4*]

[1] Department of Radiology Techniques, Mosul Medical Technical Institute, Northern Technical University, Mosul 41001, Iraq
[2] Department of Optical Techniques, College of Health and Medical Technologies, Al-Noor University, Mosul 41001, Iraq
[3] General Directorate of Nineveh Education, Iraqi Ministry of Education, Mosul 41001, Iraq
[4] Department of Animal Production Techniques, Technical Agricultural College, Northern Technical University, Mosul 41001, Iraq

Corresponding Author Email: ali.mohammed@ntu.edu.iq

https://doi.org/10.18280/ijdne.201219

Received: 13 November 2025
Revised: 19 December 2025
Accepted: 26 December 2025
Available online: 31 December 2025

Keywords:
double perovskite, $Cs_2AgBiBr_6$, lead-free, SCAPS-1D, numerical simulation, reverse illumination, photovoltaics

ABSTRACT

This study employs numerical simulation through SCAPS-1D to rigorously evaluate the performance potential of lead-free $Cs_2AgBiBr_6$ double perovskite solar cells, with three specific objectives: (1) determining the theoretical efficiency limit via systematic optimization, (2) identifying critical performance-limiting factors, particularly recombination losses, and (3) assessing the impact of illumination geometry as a secondary factor relevant to bifacial and tandem applications. By carefully changing the material properties and the device's design, a maximum power conversion efficiency (PCE) of 17.53% is reached under standard AM 1.5G lighting (open-circuit voltage (V_{OC}) = 0.887 V, short-circuit current density (J_{SC}) = 25.31 mA/cm², fill factor (FF) = 78.05%). When the light comes from the other side, the device's performance doesn't change much (< 0.4% in PCE). This shows that the direction of the light doesn't matter in structures that are symmetric and well-optimized. This is important for the designs of bifacial and tandem cells. A thorough analysis backs up the optical model and shows that the high performance is because of the effective suppression of bulk and interfacial recombination. This study sets a clear standard for performance and gives a detailed plan for how to make $Cs_2AgBiBr_6$ photovoltaics that are both efficient and good for the environment.

1. INTRODUCTION

Organic-inorganic lead halide perovskites have changed photovoltaics by making it possible to convert more than 25% of the power in just ten years [1]. But two big problems make it hard for people to use it widely: lead (Pb) is toxic on its own, and it doesn't last long in the environment [2]. The lead-free double perovskite $Cs_2AgBiBr_6$ is one of the most promising new options because it has good optoelectronic properties, such as a direct bandgap of about 1.61 eV [3], and it poses much lower risks to health and the environment. $Cs_2AgBiBr_6$ is made up of non-toxic, earth-abundant elements, is very stable in the air, and has very little effect on the environment throughout its life cycle. This makes it a good choice for next-generation photovoltaics [4, 5]. Despite these advantages, experimentally realized $Cs_2AgBiBr_6$ solar cells typically exhibit PCEs below 7% [6], far below their theoretical potential. There are a few material-level problems that cause this performance gap: (1) a relatively large bandgap (~2.0 eV) that limits absorption in the red and near-infrared spectral regions, (2) high defect densities that encourage non-radiative recombination [7], and (3) non-ideal energy alignment with common charge transport layers [8].

Drift-diffusion simulations have become an essential instrument for investigating the theoretical boundaries of innovative photovoltaic materials and directing experimental advancement [9]. This research utilizes SCAPS-1D to realize three principal research purpose: (1) ascertaining the theoretical efficiency border of $Cs_2AgBiBr_6$ solar cells via systematic optimization of material parameters and device architecture, (2) determine critical performance-limiting factors, specially centering on recombination mechanisms and interface properties, and (3) estimate the effect of illumination geometry—a pertinent factor for bifacial photovoltaics and tandem solar cell arranging where light may extract from atypical estimation.

2. MATERIAL PROPERTIES AND TOXICITY ANALYSIS

When choosing materials for green energy technologies, the environmental impact of the product over its entire life cycle must be taken into account. $Cs_2AgBiBr_6$ has a lot of good things going for it: it is not toxic, it stays stable in normal conditions, and it is made up of elements that are common on

Earth [8]. Cs2AgBiBr6 is better for the environment than lead-based perovskites and cadmium-containing thin films, but it still has the potential to perform well.

Photovoltaics made with $Cs_2AgBiBr_6$ are more environmentally friendly than those made without lead, as shown in Table 1. For instance, they make less dangerous waste when they are made, they use less energy to pay back because they can be made at low temperatures, and they might be recyclable because they are mostly made of inorganic materials [9].

Table 1. Comprehensive material properties and toxicity comparison

Material	Toxicity Level	Environmental Impact	Stability
$Cs_2AgBiBr_6$	Non-Toxic	Minimal	Excellent
MAPbI3	Highly Toxic	Severe lead contamination	Poor
FAPbI3	Highly Toxic	Severe lead contamination	Moderate
CsPbI3	Highly Toxic	Severe lead contamination	Poor
CIGS	Moderate toxicity	Cadmium concerns	Good
CdTe	Highly Toxic	Cadmium contamination	Good

3. SIMULATION METHODOLOGY AND DEVICE STRUCTURE

3.1 SCAPS-1D simulation framework

All of the numerical simulations used SCAPS-1D version 3.3.10. The software solves Poisson's equation and the continuity equations for electrons and holes at the same time when the system is in steady state [10]. It does this using computational parameters at AM 1.5G spectrum illumination (100 mW/cm², 300 K) [11]. We simulated reverse illumination by putting the light source on the back contact (CuSCN side) while keeping the device structure and optical properties the same. This method makes it possible to directly compare the effects of front and back lighting.

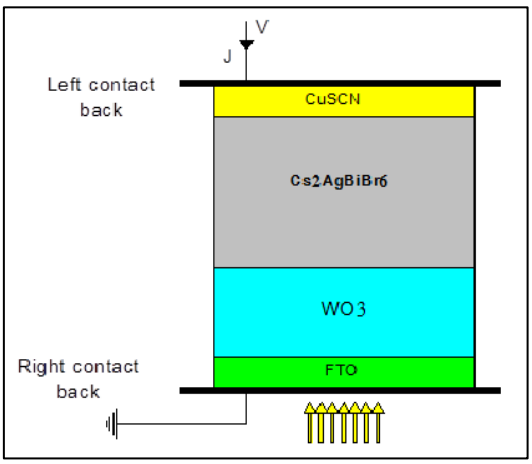

(a)

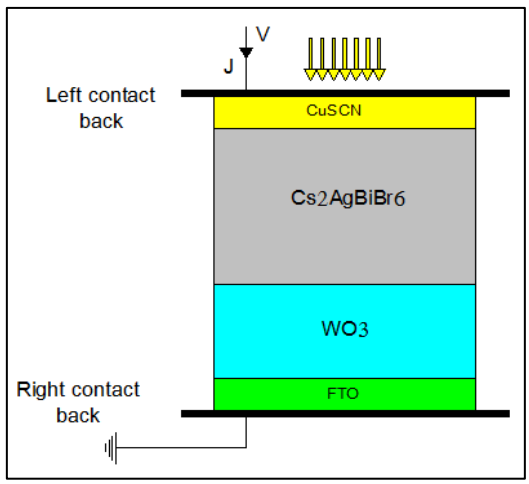

(b)

Figure 1. Schematic of the simulated solar cell structure under (a) forward and (b) reverse illumination

3.2 Device architecture and material parameters

The simulated planar n-i-p heterojunction structure is FTO/WO_3/$Cs_2AgBiBr_6$/CuSCN structure under both illumination configurations (Figure 1 and Table 2). Some parameters, such as thickness, effective density of states in the conduction and valence bands (CB and VB), shallow uniform donor density (ND), and acceptor density, were modified and changed to obtain a good working result in both directions.

Table 2. Material parameters used in the solar cell simulation

Parameter	Unit	FTO	WO_3	$Cs_2AgBiBr_6$ (Perovskite)	CuSCN
Thickness	µm	0.010	2.75	4.45	0.01
Band Gap (Eg)	eV	3.200	3.2	1.61	3.6
Electron Affinity (χ)	eV	4.400	3.8	3.72	1.7
Relative Permittivity (εr)	—	9.000	12.000	5.8	10.00
Effective DOS (CB)	1/cm³	2.20×10^{18}	2.00×10^{15}	1.00×10^{17}	2.2×10^{17}
Effective DOS (VB)	1/cm³	1.8×10^{17}	2.00×10^{14}	4.60×10^{16}	4.5×10^{19}
Electron Thermal Velocity	cm/s	1.00×10^{7}	1.00×10^{7}	1.00×10^{7}	1.00×10^{7}
Hole Thermal Velocity	cm/s	1.00×10^{7}	1.00×10^{7}	1.00×10^{7}	1.00×10^{7}
Defect Type	—	—	Neutral	Neutral	Neutral
Shallow uniform donor density (ND)	(1/cm³)	1.000×10^{10}	1.000×10^{15}	1.000×10^{2}	1.000×10^{6}
Shallow uniform acceptor density (NA)	(1/cm³)	0	0	1.000×10^{9}	2.000×10^{19}

4. RESULTS AND DISCUSSION

4.1 Current-voltage characteristics and optimal performance

Figure 2(a-b) presents the current density-voltage (J-V) characteristics of the optimized $Cs_2AgBiBr_6$ solar cell under both forward and reverse illumination conditions. The nearly overlapping curves visually demonstrate the illumination direction independence of the device performance.

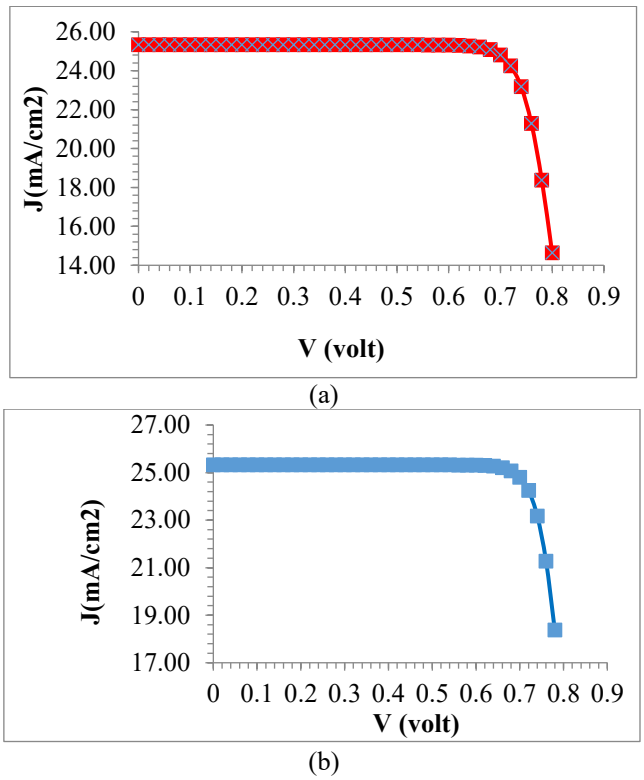

Figure 2. The current density-voltage (J-V) characteristics of the optimized $Cs_2AgBiBr_6$ solar cell under both (a) forward and (b) reverse illumination conditions

The high V_{OC} of 0.887 V corresponds to a V_{OC} deficit (E_g/q - V_{OC}) of approximately 0.723 V, comparable to high-performance lead-based perovskite devices, indicating effective suppression of non-radiative recombination pathways. The J_{SC} of 25.31 mA/cm² approaches the theoretical maximum for a 1.61 eV bandgap material, reflecting excellent light absorption and charge collection efficiencies.

4.2 Optimal device performance and illumination effects

Table 3 shows that through systematic parameter optimization, the $Cs_2AgBiBr_6$ solar cell achieves a maximum simulated PCE of 17.53% under standard test conditions.

The equivalence of the J-V characteristics under opposite illumination settings demonstrates the electrical equilibrium of the cell and its minimal dependence on illumination path, thereby approving efficient charge-carrier collection.

4.3 EQE spectrum and J_{SC} validation

The external quantum efficiency (EQE) spectrum exhibits a broad spectral response ranging from 300 nm to approximately 770 nm, with a peak value exceeding 89.8% near 660 nm (Figure 3). By integrating the EQE spectrum with the AM 1.5G photon flux, a short-circuit current density (J_{SC}) of 25.28 mA/cm² is obtained. This value is in excellent agreement with the directly simulated J_{SC} of 25.31 mA/cm², thereby validating the accuracy of the optical model.

Table 3. Performance parameters for optimized device

Configuration	V_{OC} (V)	J_{SC} (mA/cm²)	FF (%)	PCE (%)
Forward illumination	0.887	25.31	78.05	17.53
Reverse illumination	0.878	25.32	78.51	17.46
Difference	1.0%	0.04%	0.6%	0.4%

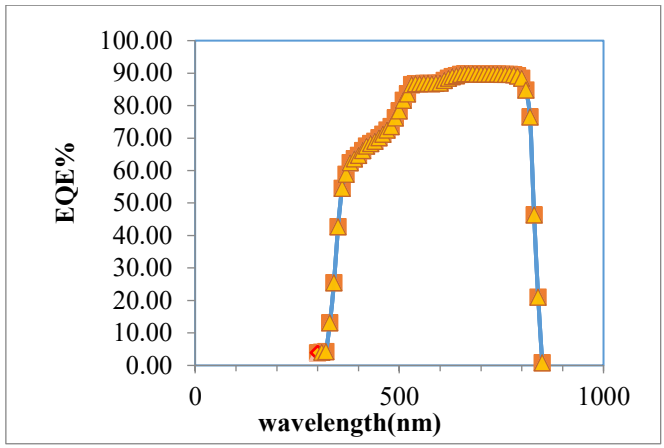

Figure 3. Simulated external quantum efficiency (EQE) spectrum of the optimized $Cs_2AgBiBr_6$ solar cell

4.4 Analysis of carrier generation and illumination direction

The optimized device architecture is symmetric, which is why the performance is almost the same in both forward and reverse illumination (0.4% PCE difference). In the idealized one-dimensional drift-diffusion model characterized by negligible parasitic absorption and equilibrated charge transport properties, symmetric device structures inherently demonstrate analogous performance irrespective of the illumination direction. The small differences we saw are probably due to numerical discretization effects, not physical asymmetries, as shown in Figure 4.

4.5 Analysis of quasi-Fermi levels and illumination symmetry

The distribution of quasi-Fermi levels for electrons and holes across the device structure was analyzed to gain insights into charge carrier transport and to assess the insensitivity of device performance to the direction of illumination. Figure 5 shows how Fermi levels are spread out in space when the lights are on. The electron Fermi level rises slowly from the front interface to the layer that absorbs light. This shows that photogeneration and electron accumulation are both working.

The electron Fermi level increases progressively from the front contact toward the light-absorbing layer, indicating efficient electron transport and photogeneration. This mode aligns with the characteristic reported for high-performing perovskite devices, which presents effective charge carriers

and reduced energy loss [12]. The whole Fermi level stays flat and close to the border of the valence band at the same time. This explains that holes can be relocated and extracted efficiently without significant energy loss at interfaces [3]. The difference between the Fermi levels of electrons and holes is directly related to the towering open-circuit voltage that can be achieved. It is also a key sign of non-radiative recombination loss [1, 12]. In our optimized structure, the maintained separation between the two levels across the device, even when illuminated from the back, signals that charge extraction is balanced and recombination is halted at both interfaces. This behavior is different from what previous studies on $Cs_2AgBiBr_6$ found, which showed that defects at the interface and energy misalignment caused strong Fermi level pinning and lower open-circuit voltage [5]. When light is shone on the FTO/WO_3/$Cs_2AgBiBr_6$/CuSCN design from both sides, the Fermi level distributions show mirror symmetry. This is similar to the generation distributions in Figure 4, which shows that the design has both structural and electronic symmetry. This symmetry keeps the internal electric field and charge collection efficiency about the same, no matter which way the light is shining. This is very substantial for bifacial and tandem solar cells, where the light can change orientation [13]. These results signalize that the intrinsic properties of lead-free double perovskite render it convenient for advanced applications [14].

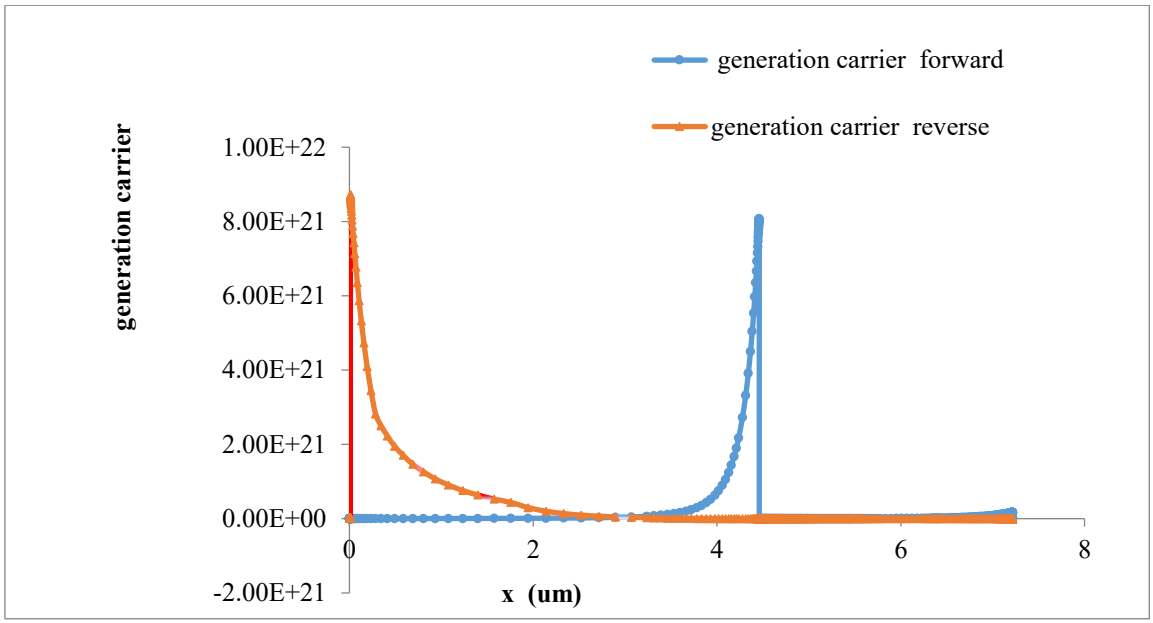

Figure 4. Spatial allocation of photogenerated transporter generation rate under forward and reverse illumination states

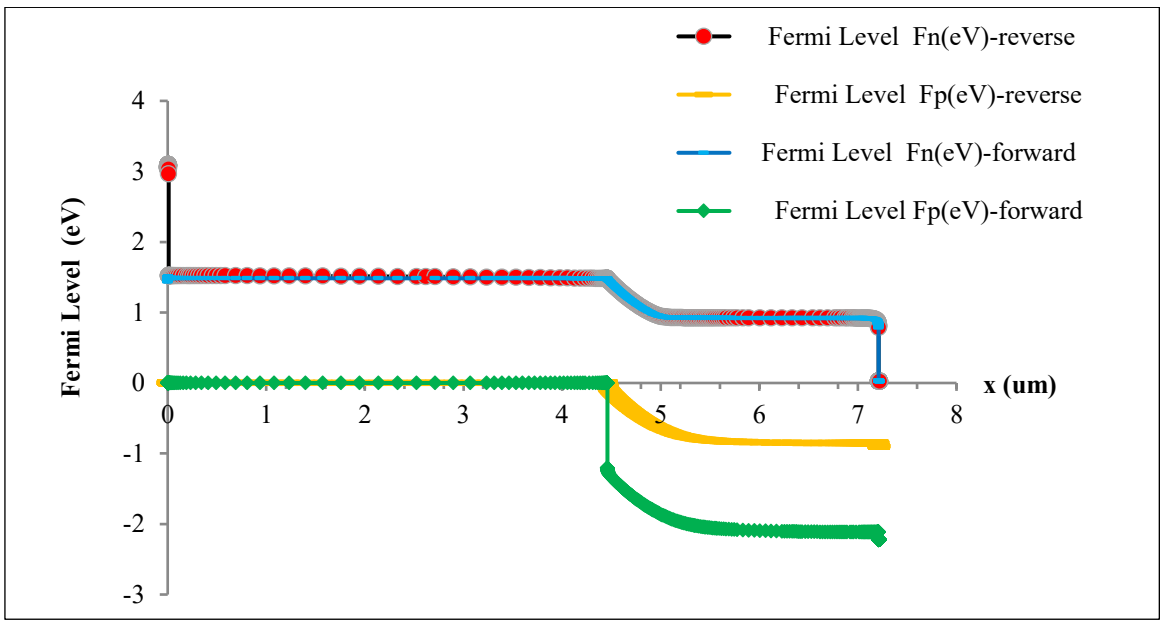

Figure 5. The spatial allocation of Fermi levels under the normal lighting state

4.6 Implications for photovoltaic applications

The statehood of the direction of light has substantial effects:

1. Bifacial photovoltaics: The corresponding performance of $Cs_2AgBiBr_6$ makes it a perfect choice for bifacial solar cells, which can capture light from both sides. This could increase energy yield by 10–30% [15].

2. Tandem solar cells: The best material for the top cell in perovskite/silicon or perovskite/perovskite tandem architectures is $Cs2AgBiBr_6$. This is because it doesn't want

light to work and has the right bandgap (1.61 eV) [13, 16].

3. Building-incorporated photovoltaics: Devices that can handle light coming from different angles give designers more options and may be able to collect more energy overall [15, 17].

4.7 Approach to theoretical optimization and model limitations

The systematic theoretical adjustment of input parameters in the SCAPS-1D simulation environment led to an optimized efficiency of 17.53%. The model's optimized key parameters were the thickness of the perovskite absorber (4.45 µm), the charge carrier mobilities, the defect density (set to a low value of $< 10^{15}$ cm^{-3}), and the band alignment at the interfaces between the electron and hole transport layers. These changes give the best result with the least amount of loss. It is important to remember that these results show a theoretical limit to performance. The sample assumes a perfect term, like perfect film morphology, a symmetrical composition, and interfaces without defects. These terms are hard to achieve in experiments. Consequently, this research sets a standard and a computational guide, emphasizing the essential material parameters that need to be regulated to reach this threshold in physical devices [18-20].

5. ENVIRONMENTAL AND SUSTAINABILITY IMPLICATIONS

Within lead-free alignment, $Cs_2AgBiBr_6$-based photovoltaics offer supplemental sustainability benefits:

- Industrial Phase: absence of toxic components. Nonattendance trash management and enriches workplace safety. Solution-processed perovskite cells employ low-temperature deposition (< 150°C) versus silicon wafer production (> 800°C), potentially decreasing embodied energy by 30-50% [21].

- Use Phase: Excellent environmental stabilization reduces encapsulation matter, lowering module weight and cost while maintaining long-term performance [4, 15].

- End-of-Life Considerations: Predominantly inorganic composition may facilitate material recovery and recycling compared to organic-inorganic hybrid perovskites [9].

6. EVALUATION OF COMPARATIVE PERFORMANCE

We compared the parameters of our simulated $Cs_2AgBiBr_6$ solar cell with those of other well-known photovoltaic technologies to put its performance into perspective, as designated in Table 4 and Figure 6.

Table 4. Performance comparison with other photovoltaic materials

Material	V_{OC} (V)	J_{SC} (mA/cm²)	FF (%)	PCE (%)
$Cs_2AgBiBr_6$	0.887	25.31	78.05	17.53
$MAPbI_3$	0.83	21.54	76.68	13.79
$FAPbI_3$	0.93	20.44	57.62	11
$CsPbI_3$	1.103	22.59	62.64	15.60
CIGS	0.741	37.8	80.6	22.6
CdTe	0.86	26.8	79	18.03

The comparison highlights several key findings. The simulated $Cs_2AgBiBr_6$ device exhibits a lower short-circuit current density (J_{SC}) compared to CIGS and CdTe, primarily due to its wider bandgap. However, it achieves a higher open-circuit voltage (V_{OC}) than most of the other photovoltaic technologies considered, with the exception of $Cs_2AgBiBr_6$. The PCE of 17.53% is similar to how well commercial thin-film technologies like CdTe work, and it is better than lead-based perovskites.

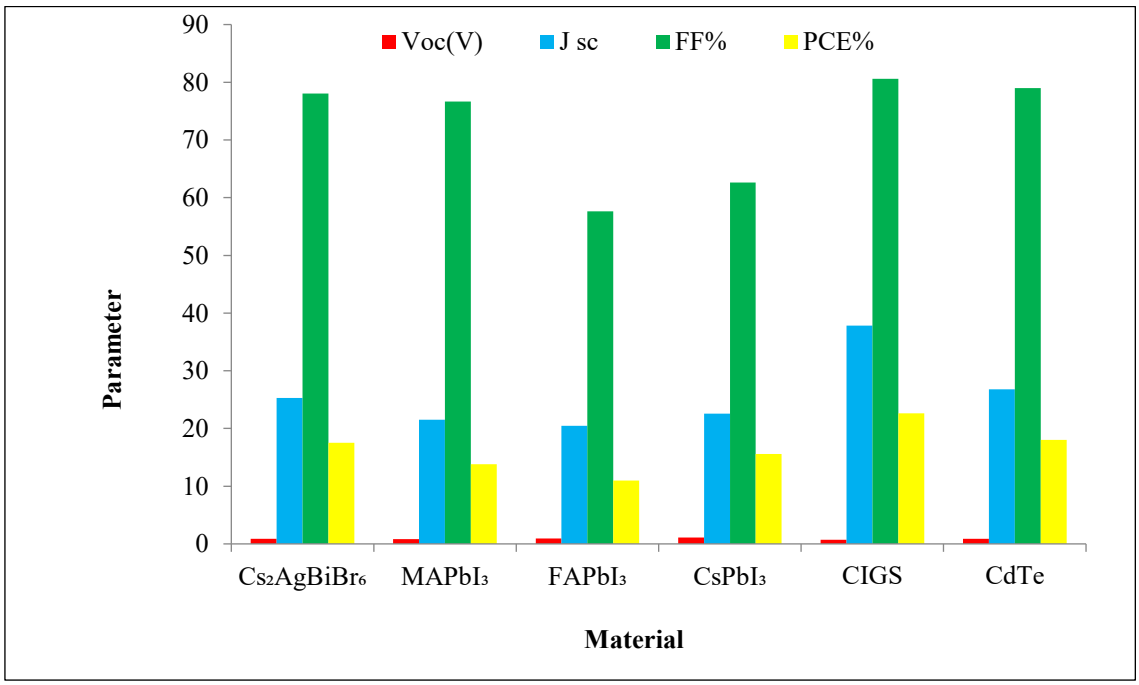

Figure 6. A bar chat comparing V_{OC}, J_{SC}, FF, and PCE of different photovoltaic materials

The $Cs_2AgBiBr_6$ device has a higher total efficiency than the $MAPbI_3$ and $FAPbI_3$ devices, even though their band gaps

are smaller. This is mostly due to the fact that the V_{OC} and FF are better. This means that lead-free double perovskite can compete with lead-based ones if the materials and the optimization of the devices are done correctly [20, 22]. The comparison with $CsPbI_3$ is very important. Our simulated $Cs_2AgBiBr_6$ device is more efficient than $CsPbI_3$ because it has a lower J_{SC} and FF, even though it has a higher V_{OC} (1.103 V). This displays how serious it is to have balanced photovoltaic properties instead of being really good at just one of them [16, 23, 24].

7. CONCLUSIONS

This overall numerical realization establishes a theoretical efficiency border of approximately 17.5% for lead-free $Cs_2AgBiBr_6$ double perovskite solar cells under optimal conditions. The simulation results significantly surpass most experimentally reported values and elucidate competitive performance compared to established photovoltaic technologies.

One important result is that the orientation of the light doesn't matter; the PCE changes by less than 0.4% between front and back lighting setups. This assist to close the gap between simulated and real-world display [12, 13, 25].

Future work should concentrate on:

1. Improving the crystals' quality to minimize the amount of bulk recombination losses [18, 26, 27].
2. Developing more effective interface engineering protocols to enhance charge extraction [18, 28, 29].
3. Investigating efficient defect passivation techniques to reduce both bulk and interface recombination [14, 25, 29].
4. Exploring advanced device architectures, such as inverted structures or graded compositions [16, 21, 30].
5. Conducting comprehensive stability testing under various environmental conditions [4, 31-33].

$Cs_2AgBiBr_6$ shows great promise for the next generation of photovoltaic technologies.

REFERENCES

[1] Jena, A. K., Kulkarni, A., Miyasaka, T. (2019). Halide perovskite photovoltaics: Background, status, and future prospects. Chemical Reviews, 119(5): 3036-3103.

[2] Shao, Y., Fang, Y., Li, T., Wang, Q., et al. (2016). Grain boundary dominated ion migration in polycrystalline organic–inorganic halide perovskite films. Energy & Environmental Science, 9(5): 1752-1759. https://doi.org/10.1039/C6EE00413J

[3] McClure, E., Ball, M., Windl, W., Woodward, P.M. (2016). Cs2AgBiX6 (X = Br, Cl): New visible light absorbing, lead-free halide perovskite. Chemistry of Materials, 28(5): 1348-1354.

[4] Hossen, M.J., Hamzah, H.M., Shahinuzzaman, M., Jamal, M.S., Said, S.M., Hatta, S.F.W.M., Miah, M.H., Khandaker, M.U., Islam, M. A. (2024). Recent progress on the efficiency and stability of lead-free $Cs_2AgBiBr_6$ double halide perovskite solar cells. Physica Scripta, 100(1): 012005. https://doi.org/10.1088/1402-4896/ad9b59

[5] Volonakis, G., Filip, M.R., Haghighirad, A.A., Sakai, N., Wenger, B., Snaith, H.J., Giustino, F. (2016). Lead-free halide double perovskites via heterovalent substitution of noble metals. The Journal of Physical Chemistry Letters, 7(7): 1254-1259.

[6] Saparov, B., Mitzi, D.B. (2016). Organic–inorganic perovskites: Structural versatility for functional materials design. Chemical Reviews, 116(7): 4558-4596.

[7] Slavney, A.H., Hu, T., Lindenberg, A.M., Karunadasa, H.I. (2016). A bismuth-halide double perovskite with long carrier recombination lifetime for photovoltaic applications. Journal of the American Chemical Society, 138(7): 2138-2141. https://doi.org/10.1021/jacs.5b13294

[8] Daem, N., Maho, A., Colson, P., Spronck, G., et al. (2025). Effect of cations substitution in lead-free double perovskite $Cs_2AgBiBr_6$ solar cells. Next Materials, 8: 100655. https://doi.org/10.1016/j.nxmate.2025.100655

[9] Burgelman, M., Decock, K., Niemegeers, A., Verschraegen, J., Degrave, S. (2016). SCAPS Manual. University of Ghent: Ghent, Belgium.

[10] Zhao, X.G., Yang, J.H., Fu, Y., Yang, D., et al. (2017). Design of lead-free inorganic halide perovskites for solar cells via cation-transmutation. Journal of the American Chemical Society, 139(7): 2630-2638.

[11] Green, M.A., Dunlop, E.D., Hohl-Ebinger, J., Yoshita, M., Kopidakis, N., Hao, X. (2021). Solar cell efficiency tables (Version 58). Progress in Photovoltaics, 29(7).

[12] Tailor, N.K., Listorti, A., Colella, S., Satapathi, S. (2023). Lead-free halide double perovskites: fundamentals, challenges, and photovoltaics applications. Advanced Materials Technologies, 8(1): 2200442. https://doi.org/10.1002/admt.202200442

[13] Baumann, S., Eperon, G.E., Virtuani, A., Jeangros, Q., Kern, D.B., Barrit, D., Schall, J., Nie, W., Oreski, G., Khenkin, M., Ulbrich, C., Peibst, R., Stein, J.S., Köntges, M. (2024). Stability and reliability of perovskite containing solar cells and modules: Degradation mechanisms and mitigation strategies. Energy & Environmental Science, 17(17): 7566-7599. https://doi.org/10.1039/D4EE02320A

[14] Domanski, K., Carlsen, B., Agrawalla, A., Alharbi, E., Graetzel, M., Hagfeldt, A., Tress, W. (2019). Performance of perovskite solar cells under real-world temperature-illumination variations in the lab. In Proceedings of the nanoGe Fall Meeting 2019.

[15] Byranvand, M.M., Saliba, M. (2021). Defect passivation of perovskite films for highly efficient and stable solar cells. Solar RRL, 5(8): 2100295.

[16] Xu, T., Xiang, W., Yang, J., Kubicki, D.J., Tress, W., Chen, T., Fang, Z., Liu, Y., Liu, S. (2023). Interface modification for efficient and stable inverted inorganic perovskite solar cells. Advanced Materials, 35(31): 2303346. https://doi.org/10.1002/adma.202303346

[17] Kamat, P.V., Bisquert, J., Buriak, J. (2017). Lead-free perovskite solar cells. ACS Energy Letters, 2(4): 904-905. https://doi.org/10.1021/acsenergylett.7b00246

[18] Park, N.G. (2020). High efficiency perovskite solar cells: Materials and devices engineering. Transactions on Electrical and Electronic Materials, 21(1): 1-15. https://doi.org/10.1007/s42341-019-00156-0

[19] Shao, M., Liu, C., Zhou, L., Xia, Y., et al. (2024). Study on the key parameters affecting the power conversion efficiency of $Cs_2AgBiBr_6$-based perovskite solar cells. Nano, 2450102. https://doi.org/10.1142/S1793292024501029

[20] Jia, L., Huang, F., Ding, H., Niu, C., et al. (2021).

Double-site defect passivation of perovskite film via fullerene additive engineering toward highly efficient and stable bulk heterojunction solar cells. Nano Today, 39: 101164.

[21] Kundu, S., Kelly, T.L. (2020). In situ studies of the degradation mechanisms of perovskite solar cells. EcoMat, 2(2): e12025. https://doi.org/10.1002/eom2.12025

[22] Tian, J., Xue, Q., Tang, X., Chen, Y., et al. (2019). Dual interfacial design for efficient $CsPbI_2Br$ perovskite solar cells with improved photostability. Advanced Materials, 31(23): 1901152. https://doi.org/10.1002/adma.201901152

[23] Kan, C., Hang, P., Wang, S., Li, B., et al. (2025). Efficient and stable perovskite-silicon tandem solar cells with copper thiocyanate-embedded perovskite on textured silicon. Nature Photonics, 19(1): 63-70. https://doi.org/10.1038/s41566-024-01561-5

[24] Li, B., Ferguson, V., Silva, S.R.P., Zhang, W. (2018). Defect engineering toward highly efficient and stable perovskite solar cells. Advanced Materials Interfaces, 5(22): 1800326. https://doi.org/10.1002/admi.201800326

[25] Al-Ashouri, A., Köhnen, E., Li, B., Magomedov, A., et al. (2020). Monolithic perovskite/silicon tandem solar cell with> 29% efficiency by enhanced hole extraction. Science, 370(6522): 1300-1309.

[26] Li, C., Wang, X., Bi, E., Jiang, F., et al. (2023). Rational design of Lewis base molecules for stable and efficient inverted perovskite solar cells. Science, 379(6633): 690-694. https://doi.org/10.1126/science.ade3970

[27] Zhao, C., Zhang, H., Krishna, A., Xu, J., Yao, J. (2024). Interface engineering for highly efficient and stable perovskite solar cells. Advanced Optical Materials, 12(7): 2301949. https://doi.org/10.1002/adom.202301949

[28] Gao, Z.W., Wang, Y., Choy, W.C. (2022). Buried interface modification in perovskite solar cells: A materials perspective. Advanced Energy Materials, 12(20): 2104030. https://doi.org/10.1002/aenm.202104030

[29] Jeong, M., Choi, I.W., Go, E.M., Cho, Y., et al. (2020). Stable perovskite solar cells with efficiency exceeding 24.8% and 0.3-V voltage loss. Science, 369(6511): 1615-1620. https://doi.org/10.1126/science.abb7167

[30] Ke, W., Kanatzidis, M.G. (2019). Prospects for low-toxicity lead-free perovskite solar cells. Nature Communications, 10(1): 965. https://doi.org/10.1038/s41467-019-08918-3

[31] Repins, I., Contreras, M.A., Egaas, B., DeHart, C., Scharf, J., Perkins, C.L., To, B., Noufi, R. (2008). 19·9 % efficient ZnO/CdS/$CuInGaSe^2$ solar cell with 81·2% fill factor. Progress in Photovoltaics: Research and Applications, 16(3): 235-239. https://doi.org/10.1002/pip.822

[32] Johnston, M.B., Herz, L.M. (2016). Hybrid perovskites for photovoltaics: Charge-carrier recombination, diffusion, and radiative efficiencies. Accounts of Chemical Research, 49(1): 146-154.

[33] Li, M., Jiao, B., Peng, Y., Zhou, J., et al. (2024). High-efficiency perovskite solar cells with improved interfacial charge extraction by bridging molecules. Advanced Materials, 36(38): 2406532. https://doi.org/10.1002/adma.202406532